



Contents lists available at ScienceDirect

## Physica D

journal homepage: [www.elsevier.com/locate/physd](http://www.elsevier.com/locate/physd)

# Analysis, simulation and visualization of 1D tapping via reduced dynamical models



Denis Blackmore<sup>a,\*</sup>, Anthony Rosato<sup>b</sup>, Xavier Tricoche<sup>c</sup>, Kevin Urban<sup>d</sup>, Luo Zou<sup>b</sup>

<sup>a</sup> Department of Mathematical Sciences and Center for Applied Mathematics and Statistics, New Jersey Institute of Technology, Newark, NJ 07102-1982, United States

<sup>b</sup> Granular Science Lab, Mechanical & Industrial Engineering Department, New Jersey Institute of Technology, Newark, NJ 07102-1982, United States

<sup>c</sup> Department of Computer Science, Purdue University, West Lafayette, IN 47907-2107, United States

<sup>d</sup> Center for Solar-Terrestrial Research, New Jersey Institute of Technology, Newark, NJ 07102-1982, United States

## HIGHLIGHTS

- A vertically tapped particle column has dynamics approximated by that of a ball.
- The dynamics can be further approximated by iterating a planar diffeomorphism.
- Simulations show the approximations are good predictors of the column dynamics.
- The efficacy of the approximations is also supported by advanced visualizations.

## ARTICLE INFO

### Article history:

Received 30 September 2013

Received in revised form

22 December 2013

Accepted 30 January 2014

Available online 7 February 2014

Communicated by V.M. Perez-Garcia

### Keywords:

Newtonian models

Center of mass model

Discrete dynamical model

Simulations

Visualizations

## ABSTRACT

A low-dimensional center-of-mass dynamical model is devised as a simplified means of approximately predicting some important aspects of the motion of a vertical column comprised of a large number of particles subjected to gravity and periodic vertical tapping. This model is investigated first as a continuous dynamical system using analytical, simulation and visualization techniques. Then, by employing an approach analogous to that used to approximate the dynamics of a bouncing ball on an oscillating flat plate, it is modeled as a discrete dynamical system and analyzed to determine bifurcations and transitions to chaotic motion along with other properties. The predictions of the analysis are then compared – primarily qualitatively – with visualization and simulation results of the reduced continuous model, and ultimately with simulations of the complete system dynamics.

© 2014 Elsevier B.V. All rights reserved.

## 1. Introduction

Continuing our work in [1], we delve even more deeply into the dynamics of a vertically tapped column of particles; this time exploring how certain “averaged” approximations can yield useful information about the dynamics of the complete system such as the identification of a key dimensionless bifurcation parameter related to the acceleration of the tap that signals period-doubling cascades and transitions to chaos. The underlying idea or theme in using such approximate models is that the loss in accuracy may be

more than compensated for by enhanced amenability to detailed mathematical analysis. In particular, we focus on the dynamics of the center of mass of the particle configuration as it evolves under the action of gravity and the periodic tapping force applied via the floor (bottom) of the configuration, which can be approximated by a two-degree-of-freedom system that is essentially ‘equivalent’ to a single ball driven by the oscillatory motion of the floor (as borne out by qualitative comparisons with simulations of the complete system). Naturally, one cannot expect that the motion of the center of mass is capable of illuminating many of the more subtle aspects of the dynamics of the complete system; however, it is plausible that transitions to chaotic regimes can be rather well predicted by the reduced system. The reason for this is that chaotic motions of individual particles would typically not cancel one another in the averaging that defines the position of the center of mass, and the dynamics of the center of mass cannot possibly be chaotic

\* Corresponding author.

E-mail addresses: [deblac@m.njit.edu](mailto:deblac@m.njit.edu) (D. Blackmore), [anthony.rosato@njit.edu](mailto:anthony.rosato@njit.edu) (A. Rosato), [xmt@purdue.edu](mailto:xmt@purdue.edu) (X. Tricoche), [kdu2@njit.edu](mailto:kdu2@njit.edu) (K. Urban), [lz39@njit.edu](mailto:lz39@njit.edu) (L. Zou).

unless the same is true for at least one of the particles in the complete system. What we found to be most surprising is that the reduced (center of mass) dynamics appears to be a reasonably good bellwether for other types of changes in the qualitative dynamics such as period-doubling bifurcations and is rather useful for characterizing other dynamical phenomena for the complete system such as the existence of periodic orbits of arbitrarily large period as well as (what appear to be) strange attractors.

We begin in Section 2 with a continuous one-dimensional dynamical model for the vertical column of particles (assuming a modified Walton–Braun type interaction law with different spring constants for loading and unloading [2,3] and an impulse-like oscillatory motion for the floor). The governing equations for the motion of the column of particles are then expressed as a system of second-order ordinary differential equations (ODEs) in the usual Newtonian way (and the initial equilibrium configuration of the particle stack is derived) and this is recast as a system of first-order equations in the standard manner. In these systems, the role of inelasticity (which causes dissipation in the dynamics) is highlighted and quantified by a parameter that is directly related to the coefficient of restitution, which is the more familiar measure of energy loss in the particle–particle and particle–floor interactions. It is interesting and instructive to compare our modeling and analysis with such related investigations as [4–19].

In Section 3, we use the equations of motion of the complete system to determine the reduced governing equations for the dynamics of the center of mass. Taking full advantage of Newton's third law of motion, we show that these reduced equations make it possible to uniquely determine the dynamics of the mass center by a single second-order ODE if the motion of the particle nearest the floor is known. Whence, the assumption of a reasonable relationship between the motion of the particle nearest the floor and the center of mass (which becomes more accurate as the number of particles increases) enables us to approximate the motion of the center of mass by a second-order ODE that is equivalent to a single ball bouncing on the oscillating floor—albeit a ball with mass equal to the total mass of particles in the full system that is acted upon by a suitably modified gravitational force. It should be noted here that the apparent relationship between the bouncing ball and oscillating granular column dynamics was observed about a decade ago, empirically justified, investigated in some detail and more or less confirmed via simulation by Luding et al. [20,21] and Brennen et al. [22]. An inescapable and quite interesting inference that one perforce draws from this equivalence is that the dynamics of the center of mass is at least as rich and varied as that of a ball bouncing on a vibrating plate (as delineated in such studies as [23–26]).

Next, in Section 4, we further simplify our reduced continuous model for the evolution of the center of mass using two discrete dynamical system approximations that rather accurately portray certain key features of the motion of the reduced center of mass model. The first discrete dynamical systems model is developed along the lines formulated by Holmes [24], and also turns out to be basically equivalent to the *standard map* [24,27–29]. We perform an in-depth analysis of dynamics of this model that reveals that there is an acceleration-(or energy-) like non-dimensional parameter that governs transitions from regular motions to period-doubling bifurcations and ultimately to chaotic dynamics; it is the same parameter that has been shown to play a pivotal role in bifurcations of bouncing-ball dynamics and (via simulation and experiments) the motion of the complete stack of particles.

Section 5 is devoted to wide-ranging simulations of the dynamics of a tapped column of a large number of particles (computing the trajectories of the individual particles) and the corresponding motion of the center of mass of the configurations. These simulations – performed using a very effective granular

dynamics based code that has been refined and upgraded over several years (cf. [1,7,15,30,31]) – are focused on observing how the complete system and center of mass reductions respond to changes in several important parameters, both physical and non-dimensional, with an eye toward comparisons with predictions from the analytical investigation in the preceding sections. It is found that there is rather good agreement between the analytical and computational results.

In addition to establishing agreement between the analytical and simulation aspects of our investigation, in Section 6 we include comparisons of the reduced center of mass motion results with conclusions obtained using dynamical visualization techniques such as those described in [32–35]. In particular, appropriate phase space visualization methods are used on the continuous second-order ODE model selected to approximate the dynamics of the center of mass of the configuration. These methods typically involve the identification of several types of coherent phase space structures that have been found to correspond to various dynamical regimes and transitions among them. Comparisons at several levels for numerous parameter values reveal remarkably good qualitative agreement among the analysis, simulation and visualization approaches, thereby confirming the effectiveness of this tripartite strategy for dynamical investigations.

Finally, in Section 7, we conclude with a succinct summary of the results obtained and their importance in this and related investigations. Moreover, we briefly outline our plans for future studies inspired by our work here—directed mainly at useful alternative reduced models and extensions to higher dimensions and generalization of the systems considered.

## 2. Newtonian model

First, we derive the equations of motion for a vertically tapped column of particles using Newtonian and Hamiltonian principles assuming that the particle–particle and particle–floor interaction forces are of a modified simplified Walton–Braun (W–B) type (cf. [5,6,12,16,36]). A simplified type of W–B model is employed to avoid the extra calculations associated with the initiation of interactions in progress at any given time. It should be noted that the modification does not alter the particle (mass center) dynamics, because both models yield precisely the same velocities before and after contact (related to the coefficient of restitution).

To be precise, we consider a vertical configuration of  $N$  particles  $p_i$ ,  $1 \leq i \leq N$ , stacked one above the other starting with  $p_1$ , under the action of gravity – with constant gravitational acceleration  $g$  – and interacting inelastically (according to the modified W–B model) with neighboring particles and the rigid bottom. The bottom (floor) of the stack, denoted as  $y_0$  and initially at zero, moves so as to simulate a periodic nearly impulsive force applied vertically to the floor. The floor and particle centers are located, respectively, at the points

$$0 \leq y_0(t) < y_1 < \dots < y_N \quad (1)$$

in  $I := \{y : 0 \leq y\}$ , and we assume that the particles have masses and radii  $m_1, r_1, \dots, m_N, r_N$ , respectively.

We assume that  $y_0(t)$  is a periodic function of period  $T > 0$  represented as

$$y_0(t) := \begin{cases} a \sin \omega t, & 0 \leq t \leq \pi/\omega \\ 0, & \pi/\omega \leq t \leq T \end{cases} \quad (2)$$

for  $0 \leq t \leq T$ , where  $\pi/\omega \ll T$ , and the amplitude  $a$  is small and positive. The derivative of  $y_0$  with respect to  $t$ ,  $\dot{y}_0$ , is the discontinuous function

$$\dot{y}_0(t) := \begin{cases} a\omega \cos \omega t, & 0 \leq t \leq \pi/\omega \\ 0, & \pi/\omega \leq t \leq T. \end{cases} \quad (3)$$

In our analysis of the dynamics in the sequel, we shall find it necessary to smoothen the above motion (by rounding the corners) so that  $y_0$  can be considered to be a  $C^2$  function and *a fortiori*  $\dot{y}_0$  can be treated as a  $C^1$  function. This can be accomplished with arbitrarily close  $C^0$  approximations, so the overall dynamics of the original and smoothed systems are essentially the same.

The particles and bottom are assumed to interact (inelastically) according to a simplified version of the W–B law, so that the equations of motion obtained from Newton's laws are the following system of  $N$  second-order ordinary differential equations (ODEs):

$$m_i \ddot{y}_i = F_i, \quad (1 \leq i \leq N) \quad (4)$$

where the forces on the particles are

$$F_i := -m_i g + f_i^{i-1} + f_i^{i+1} \quad (5)$$

for  $1 \leq i \leq N$ , where  $f_i^{i-1}$  is the force exerted by  $p_{i-1}$  (or the floor when  $i = 1$ ) on  $p_i$  and  $f_i^{i+1}$  is the force exerted by  $p_{i+1}$  on  $p_i$  when  $1 \leq i \leq N - 1$ . These interaction forces are assumed to have the form (cf. [1])

$$\begin{aligned} f_1^0 &:= K_1^0 [1 - \varepsilon_{0,1} \sigma (\dot{y}_1 - \dot{y}_0(t))] [r_1 - (y_1 - y_0(t))] \\ &\quad \times \chi (r_1 - (y_1 - y_0(t))) \mathfrak{F} (|y_1 - y_0(t)|, \dot{y}_1 - \dot{y}_0(t)), \\ f_i^{i+1} &:= -K_i^{i+1} [1 - \varepsilon_{i,i+1} \sigma (\Delta \dot{y}_i)] [r_i + r_{i+1} - \Delta y_i] \\ &\quad \times \chi (r_i + r_{i+1} - \Delta y_i) \mathfrak{F} (|\Delta y_i|, \Delta \dot{y}_i), \end{aligned} \quad (6)$$

$$f_N^{N+1} := 0,$$

for  $1 \leq i \leq N - 1$ , with

$$f_i^{i-1} = -f_{i-1}^i \quad (7)$$

for  $2 \leq i \leq N$ . Here

$$\begin{aligned} \Delta y_i &:= y_{i+1} - y_i, \\ \Delta \dot{y}_i &:= \dot{y}_{i+1} - \dot{y}_i, \end{aligned} \quad (8)$$

for  $1 \leq i \leq N - 1$ ,  $K_i^0$  and  $K_i^{i+1}$  are positive constants, the interaction coefficients  $0 \leq \varepsilon_{i,i+1} < 1$  for all  $0 \leq i \leq N - 1$ ,  $\sigma$  and  $\chi$  denotes the signum and step function defined, respectively, by

$$\sigma(\tau) := \begin{cases} -1, & \tau < 0 \\ 0, & \tau = 0 \\ 1, & \tau > 0 \end{cases} \quad \text{and} \quad \chi(\tau) := \begin{cases} 0, & \tau \leq 0 \\ 1, & \tau > 0 \end{cases} \quad (9)$$

and  $\mathfrak{F} : (0, \infty) \rightarrow [1, \infty)$  is a continuous penalty function added to make sure that the material properties of the system cannot be violated. In particular, particles should not be able to pass through one another nor through the floor of the stack. In order to adhere reasonably closely to the linear spring model, we define this function as

$$\mathfrak{F}(\tau, \nu) := 1 + \chi(-\nu) \chi(\tau_* - \tau) \left[ 1 + \frac{1}{\sqrt{\tau}} - \frac{1}{\sqrt{\tau_*}} \right], \quad (10)$$

where  $\tau_* := \min\{r_i : 1 \leq i \leq N\}/100$ . The penalty function is only activated when the particles (or a particle and the floor) are approaching and extremely deformed so as not to unduly affect the actual physical interactions being modeled. We found that this penalty function works quite well for the type of mild taps on which we are concentrating, but more energetic taps require a stronger penalty function in which  $\tau^{-1/2}$  is replaced by  $\tau^{-\alpha}$  with  $\alpha \geq 1$  (see e.g. [37]).

With the definitions above, the system (4) may now be rewritten as

$$\ddot{y}_i = Y_i := \frac{1}{m_i} F_i = -g + \frac{1}{m_i} (f_i^{i-1} + f_i^{i+1}), \quad (1 \leq i \leq N) \quad (11)$$

which can be recast in vector form for  $\mathbf{y} := (y_1, \dots, y_N)$  as

$$\ddot{\mathbf{y}} = \mathbf{Y}(\mathbf{y}, \dot{\mathbf{y}}, t; \mu), \quad (12)$$

where  $\mathbf{Y} := (Y_1, \dots, Y_N) = (-g + m_1^{-1}(f_1^0 + f_1^2), \dots, -g + m_{N-1}^{-1}(f_{N-1}^{N-2} + f_{N-1}^N), -g + m_N^{-1}f_N^{N-1})$ , and  $\mu$  is a parameter (vector) incorporating  $a, \omega, T$ , all the particle masses and radii, and all of the interaction parameters  $K_i^{i+1}$  and  $\delta_{i,i+1}$ . As is usual for such second-order systems, it is often convenient to recast it as the following system of  $2N$  first-order ODEs:

$$\begin{aligned} \dot{y}_i &= z_i, \\ \dot{z}_i &= Y_i, \end{aligned} \quad (13)$$

for  $1 \leq i \leq N$ . This can also be represented in vector form as

$$\dot{\mathbf{x}} = \mathbf{X}(\mathbf{x}, t; \mu), \quad (14)$$

where  $\mathbf{x} := (y_1, \dot{y}_1, \dots, y_N, \dot{y}_N)$ .

For the above forces the inelasticity of the particle–particle and particle–bottom interactions is manifested by a loss of energy upon impact that is represented by a spring constant of  $K_i^{i+1} (1 + \varepsilon_{i,i+1})$  when the objects are approaching one another or the bottom and a spring constant of  $K_i^{i+1} (1 - \varepsilon_{i,i+1})$  in separation, so the energy stored in unloading is smaller than that in loading by a factor of  $(1 - \varepsilon_{i,i+1}) (1 + \varepsilon_{i,i+1})^{-1}$ . Hence,  $\varepsilon_{i,i+1} = 0$  represents a perfectly elastic interaction. We also note that although the discontinuities in (12) or (14) are somewhat inconvenient from a theoretical standpoint, they can easily be handled by a standard numerical scheme, such as a Runge–Kutta solver, and the forces can also be  $C^0$ -approximated to any degree of accuracy by smooth ( $=C^\infty$ ) functions.

The initial conditions for (14) consistent with tapping are given in vector form as

$$\mathbf{x}(0) = (y_1(0), 0, y_2(0), \dots, 0, y_N(0), 0), \quad (15)$$

which represents a stacked configuration of particles initially at rest. Here we have to determine the values of the  $y_k(0)$  by requiring that the stack of particles is initially at rest and in equilibrium. As the particles are assumed to be non-rigid we shall have to determine these values in a way that guarantees that  $y_0(0) < y_1(0) < y_2(0) < \dots < y_N(0)$ , which we shall demonstrate in the sequel.

We shall simplify matters by assuming from here on that all the  $K$ 's and all the  $\varepsilon$ 's are equal. Note that in this context, the coefficient of restitution  $e$ , which is the standard measure of elasticity (where  $0 \leq e \leq 1$ , with  $e = 0$  and  $e = 1$  representing the perfectly inelastic and elastic cases, respectively), is given as [2,3]

$$e = \sqrt{\frac{1 - \varepsilon}{1 + \varepsilon}} \iff \varepsilon = \frac{1 - e^2}{1 + e^2}. \quad (16)$$

With the assumptions that all  $K$ 's and  $e$ 's are the same, the equations of motion take the form

$$\ddot{y}_i = Y_i := -g + \frac{1}{m_i} (f_i^{i-1} + f_i^{i+1}), \quad (1 \leq i \leq N) \quad (17)$$

where

$$\begin{aligned} f_1^0 &:= K [1 - \varepsilon \sigma (\dot{y}_1 - \dot{y}_0(t))] [r_1 - (y_1 - y_0(t))] \\ &\quad \times \chi (r_1 - (y_1 - y_0(t))) \mathfrak{F} (|y_1 - y_0(t)|, \dot{y}_1 - \dot{y}_0(t)), \\ f_i^{i+1} &:= -K [1 - \varepsilon \sigma (\Delta \dot{y}_i)] [r_i + r_{i+1} - \Delta y_i] \\ &\quad \times \chi (r_i + r_{i+1} - \Delta y_i) \mathfrak{F} (|\Delta y_i|, \Delta \dot{y}_i), \\ f_N^{N+1} &:= 0. \end{aligned} \quad (18)$$

Whence, the Newtonian equations of motion are

$$\begin{aligned}\ddot{y}_1 &= -g - \frac{K}{m_1} \{ [1 - \varepsilon\sigma(\Delta\dot{y}_1)] [r_1 + r_2 - \Delta y_1] \\ &\quad \times \chi(r_1 + r_2 - \Delta y_1) \mathfrak{F}(|\Delta y_1|, \Delta\dot{y}_1) \\ &\quad - [1 - \varepsilon\sigma(\dot{y}_1 - \dot{y}_0(t))] [r_1 - (y_1 - y_0(t))] \\ &\quad \times \chi(r_1 - (y_1 - y_0(t))) \mathfrak{F}(|y_1 - y_0(t)|, \dot{y}_1 - \dot{y}_0(t)) \}, \\ \ddot{y}_i &= -g - \frac{K}{m_i} \{ [1 - \varepsilon\sigma(\Delta\dot{y}_i)] [r_i + r_{i+1} - \Delta y_i] \\ &\quad \times \chi(r_i + r_{i+1} - \Delta y_i) \mathfrak{F}(|\Delta y_i|, \Delta\dot{y}_i) \\ &\quad - [1 - \varepsilon\sigma(\Delta\dot{y}_{i-1})] [r_{i-1} + r_i - \Delta y_{i-1}] \\ &\quad \times \chi(r_{i-1} + r_i - \Delta y_{i-1}) \mathfrak{F}(|\Delta y_{i-1}|, \Delta\dot{y}_{i-1}) \}, \\ \ddot{y}_N &= -g + \frac{K}{m_N} [1 - \varepsilon\sigma(\Delta\dot{y}_{N-1})] [r_{N-1} + r_N - \Delta y_{N-1}] \\ &\quad \times \chi(r_{N-1} + r_N - \Delta y_{N-1}) \mathfrak{F}(|\Delta y_{N-1}|, \Delta\dot{y}_{N-1}),\end{aligned}\quad (19)$$

with initial conditions

$$y_1(0), \dots, y_N(0) \text{ determined by assuming} \\ \text{initial equilibrium, and } \dot{y}_1(0) = \dots = \dot{y}_N(0) = 0. \quad (20)$$

To determine the initial positions of the particle centers, we simply set  $y_0, \dot{y}_0$  and  $\dot{y}_i$  and  $\dot{y}_i$  ( $1 \leq i \leq N$ ) equal to zero and assume all  $|\Delta y_i| > \tau_*$ , which yields the linear system

$$\begin{aligned}-2y_1(0) + y_2(0) &= r_2 + \frac{m_1 g}{K}, \\ y_{k-1}(0) - 2y_k(0) + y_{k+1}(0) &= (r_{k+1} - r_{k-1}) + \frac{m_k g}{K}, \\ (1 < k < N - 1) \\ y_{N-1}(0) - y_N(0) &= -(r_{N-1} + r_N) + \frac{m_N g}{K}.\end{aligned}\quad (21)$$

It is straightforward to show that (21) has the solution

$$\begin{pmatrix} y_1(0) \\ y_2(0) \\ y_3(0) \\ \vdots \\ y_{N-1}(0) \\ y_N(0) \end{pmatrix} = \begin{pmatrix} -1 & -1 & -1 & -1 & \dots & -1 \\ -1 & -2 & -2 & -2 & \dots & -2 \\ -1 & -2 & -3 & -3 & \dots & -3 \\ \vdots & \vdots & \vdots & \vdots & \dots & \vdots \\ -1 & -2 & -3 & \dots & -(N-1) & -(N-1) \\ -1 & -2 & -3 & -4 & \dots & -N \end{pmatrix} \times \begin{pmatrix} r_2 + \frac{m_1 g}{K} \\ r_3 - r_1 + \frac{m_2 g}{K} \\ r_4 - r_2 + \frac{m_3 g}{K} \\ \vdots \\ r_N - r_{N-2} + \frac{m_{N-1} g}{K} \\ -(r_{N-1} + r_N) + \frac{m_N g}{K} \end{pmatrix}, \quad (22)$$

which satisfies the requirement that  $y_k(0) - y_{k-1}(0) > 0$  for all  $1 \leq k \leq N$  if

$$K > \frac{1}{10g} \max \left\{ \frac{m_k}{r_{k-1} + r_k} : 1 \leq k \leq N \right\}, \quad (23)$$

where we have defined  $r_0 = 0$  for convenience. We note here that the maximum height  $h_{\max}$  of the column of particles – where they are all just touching one another – is

$$h_{\max} = 2(r_1 + r_2 + \dots + r_N). \quad (24)$$

We shall study the solutions of (19)–(20). One slightly troubling feature from a theoretical standpoint is the fact is that the forces and their derivatives have discontinuities, which we should add can be easily handled using a numerical scheme such as the Runge–Kutta method. Theoretically, we can always adjust the systems to be smooth ( $=C^\infty$ ) by using appropriate approximations of the signum, step and penalty functions. Rather good choices for smooth approximations of  $\sigma$  and  $\chi$  are

$$\begin{aligned}\sigma(s) &\cong \sigma_\alpha(s) := \tanh \alpha s \quad \text{and} \\ \chi(s) &\cong \chi_\alpha(s) := \frac{1}{2} (1 + \tanh \alpha s),\end{aligned}\quad (25)$$

where  $\alpha \gg 1$ , while the penalty function  $\mathfrak{F}$  can be smoothed at  $s = \tau_*$  and smoothly capped off at a very high value at  $s = 0$ .

### 3. Reduced center of mass model

The initial value problem (19)–(20) is difficult to analyze or visualize even for moderate values of  $N$  since it is highly nonlinear. On the other hand, this initial value problem (IVP) can be handled easily – at least in principle – using numerical techniques such as the standard 4th-order Runge–Kutta method or better yet a sophisticated discrete element simulation code such as that employed in [15]. However, even the best simulation method for obtaining approximate solutions tends to become too computationally expensive for very large values of  $N$ . For these reasons, it would prove quite useful to have a model of a significantly smaller dimension that is capable of capturing or approximating important features of the motion of the full system, yet is still far more amenable to mathematical analysis, numerical solution and the application of dynamical visualization techniques such as those employed in [32–35]. We shall develop such a reduced dynamical model here—one based on the motion of the center of mass of the particle stack.

Let us first define the coordinate of the center of mass of the stack as

$$\bar{y} := \frac{1}{M} \sum_{k=1}^N m_k y_k, \quad (26)$$

where  $M := m_1 + m_2 + \dots + m_N$ . Then it follows directly from (19)–(20) that  $\bar{y}$  is the solution of the IVP

$$\begin{aligned}\ddot{\bar{y}} &= -g + \frac{K}{M} [1 - \varepsilon\sigma(\dot{y}_1 - \dot{y}_0(t))] [r_1 - (y_1 - y_0(t))] \\ &\quad \times \chi(r_1 - (y_1 - y_0(t))) \mathfrak{F}(|y_1 - y_0(t)|, \dot{y}_1 - \dot{y}_0(t))\end{aligned}\quad (27)$$

$$\bar{y}(0) = \frac{1}{M} \sum_{k=1}^N m_k y_k(0), \quad \dot{\bar{y}}(0) = 0, \quad (28)$$

where  $y_1(0), \dots, y_N(0)$  are determined by (22), and Newton's 3rd law has been used to great advantage in obtaining the rather simple form of the differential equation that is a “reduction” from a system of  $N$ , 2nd-order equations to a single 2nd-order equation. As  $\bar{y}(t) \neq y_1(t)$  unless  $N = 1$ , (27) is not a, strictly speaking, differential equation for  $\bar{y}$  and naturally not the kind of reduced center of mass model we seek. However, it does lead directly to the following rather surprising result.

**Lemma 1.** *The motion of the center of mass of the vertical array of particles governed by the system of second-order differential*

equations (19) is completely determined by the motion,  $y_1(t)$ , of the particle nearest the floor of the column.

In order to turn (27) into a precise reduced differential equation for the motion of the center of mass, we must know in advance the relationship between  $y_1$  and  $\bar{y}$  for all time; but this is only possible if we first solve the whole system IVP (19)–(20). As this defeats its own purpose, we shall find an “approximating” reduction by simply making a plausible guess about the relationship. One of the simplest reasonable assumptions is the following:

$$y_1 \cong \frac{\bar{y}}{N}.$$

Consequently, we take our approximate reduced model of the IVP (27)–(28), with  $z$  approximating  $\bar{y}$ , to be

$$\ddot{z} = -g + \frac{K}{M} \left[ 1 - \varepsilon \sigma \left( \frac{\dot{z}}{N} - \dot{y}_0(t) \right) \right] \left[ r_1 - \left( \frac{z}{N} - y_0(t) \right) \right] \\ \times \chi \left( r_1 - \left( \frac{z}{N} - y_0(t) \right) \right) \mathfrak{F} \left( \left| \frac{z}{N} - y_0(t) \right|, \frac{\dot{z}}{N} - \dot{y}_0(t) \right), \quad (29)$$

$$z(0) = \frac{1}{M} \sum_{k=1}^N m_k y_k(0), \quad \dot{z}(0) = 0, \quad (30)$$

and simply remark that there are other plausible choices such as

$$y_1 = \frac{\bar{y}}{N} (1 + y_0(t))$$

that might also be worth trying. At any rate, it is not unreasonable to assume that certain features of the dynamics of (29), such as bifurcations and transitions from regularity to chaos, can (approximately) signal the same behaviors in the full system (19).

One of the nicest features of the reduced model is that it is more amenable to visualization inasmuch as its solution can be viewed in terms of time-varying orbits of the  $T$ -periodic, planar dynamical system in the usual variables  $(\xi, \eta) := (z, \dot{z})$

$$\dot{\xi} = \eta, \\ \dot{\eta} = -g + \frac{K}{M} \left[ 1 - \varepsilon \sigma \left( \frac{\eta}{N} - \dot{y}_0(t) \right) \right] \left[ r_1 - \left( \frac{\xi}{N} - y_0(t) \right) \right] \\ \times \chi \left( r_1 - \left( \frac{\xi}{N} - y_0(t) \right) \right) \mathfrak{F} \left( \left| \frac{\xi}{N} - y_0(t) \right|, \frac{\eta}{N} - \dot{y}_0(t) \right), \quad (31)$$

which can also be recast in the usual fashion (by taking  $t$  to be a third dependent variable) as an autonomous dynamical system in  $\mathbb{R}^3$ . In fact, it follows from the periodicity that the phase space can actually be reduced to  $\mathbb{R}^2 \times \mathbb{S}^1$ , where  $\mathbb{S}^1$  is the unit circle. It should be remarked that if (31) is solved by a one-step numerical method such as the standard Runge–Kutta scheme, one generally encounters difficulties when  $\xi$  is small and  $-\eta$  is large. Therefore, it is helpful to use a variable time step in such cases that is chosen along the following lines: If  $0 \leq \xi \leq 4r_1$  and  $\eta < 0$ , select the time step to satisfy

$$\Delta t \leq \xi/5 |\eta|,$$

so as to avoid numerical difficulties and problems of physical inconsistency such as the point representing the center of the object penetrating the floor of the system.

Observe that the system (29)–(30) looks very much like that associated with a bouncing ball on an oscillating table, which has been the subject of considerable research (see e.g. [24,26,27]). Thus it is reasonable to assume that some of the techniques that have illuminated a wide range of dynamic behaviors for the bouncing ball problem can be adapted to uncover analogous results for (29). One of these approaches, pioneered by Holmes [24], the reformulation of the equations as a discrete dynamical system, shall be investigated in the next section.

#### 4. Discrete dynamical models of reduced system

In this section we describe a couple of ways in which (29)–(30) can be recast as a discrete dynamical system. We then analyze these discrete formulations to determine some important features of the continuous system from whence they deduced. Our first discrete dynamical model is completely analogous to that of Holmes for a single particle, thereby enabling us to directly infer a host of dynamical properties from the results in [24]. It should be noted that the continuous dynamical system corresponding to this discrete model also enables us to predict that the center of mass motion exhibits the full range of dynamics known to exist for a single bouncing ball such as shown in [23,25,26].

##### 4.1. Discrete model of Holmes type

In order to show how to fully exploit the Holmes' standard map model, we first compare the Newtonian dynamical equations for a single particle with (29) assuming that the interaction force models are the same for both. In the case of a single particle of mass  $m$ , radius  $r$  and coefficient of restitution  $e = \sqrt{(1-\varepsilon)/(1+\varepsilon)}$  it is easy to see upon comparison with (29) that the governing equation for the motion of the center of mass of the particle is

$$\ddot{y} = -g + \frac{K}{m} [1 - \varepsilon \sigma (\dot{y} - \dot{y}_0(t))] [r - y + y_0(t)] \\ \times \chi (r - y + y_0(t)) \mathfrak{F} (|y - y_0(t)|, \dot{y} - \dot{y}_0(t)). \quad (32)$$

For purposes of comparison, we rewrite (29) as

$$\ddot{y}_* = -g_* + \frac{K}{m_*} [1 - \varepsilon \sigma (\dot{y}_* - \dot{y}_0(t))] [r - y_* + y_0(t)] \\ \times \chi (r - y_* + y_0(t)) \mathfrak{F} (|y_* - y_0(t)|, \dot{y}_* - \dot{y}_0(t)), \quad (33)$$

where

$$y_* := \frac{z}{N}, \quad g_* := \frac{g}{N} \quad \text{and} \quad m_* := MN.$$

Hence, the dynamics of (29), or equivalently (31), is identical to that of a single ball of mass  $m_*$ , radius  $r$  and coefficient of restitution  $e = \sqrt{(1-\varepsilon)/(1+\varepsilon)}$  bouncing on a table vibrating according to (2) in a gravitational field with acceleration  $g_*$  (where it should be noted that the velocity of the table in the new coordinate  $y_*$  is  $\dot{y}_0/N$ ). Consequently, the myriad results on the continuous dynamics of a single bouncing ball exemplified by investigations such as [23,25,26], after the obvious adjustments in form, apply to our reduced (center of mass) system. This of course includes such phenomena as period-doubling bifurcations, transitions to chaos and existence of strange attractors for certain parameter ranges.

The analogy for continuous dynamics carries over also to the discrete approximation used by Holmes to investigate the dynamics of a bouncing ball. In fact, if we adopt the same assumptions and follow the same procedure as Holmes [24], it is straightforward to show that the (nondimensionalized) map

$$\Phi : \mathbb{S}^1 \times \mathbb{R} \rightarrow \mathbb{S}^1 \times \mathbb{R}, \\ \Phi (\theta, v) := ([\theta + v], ev + \gamma W(\theta + v)), \quad (34)$$

where  $[\cdot]$  denotes the congruence class mod  $\omega T$ , generates a discrete dynamical system that closely approximates the times  $t_n$  and velocities  $V_n$  of successive impacts of the “ball” of (33) with the vibrating floor. Here,  $\theta := \omega t$ ,  $v := 2\omega V/g_*$ ,  $\gamma := (2a\omega^2/N)(1+e)/g_* = 2a\omega^2(1+e)/g$  and  $W$  is a  $\omega T$ -periodic function defined on a period interval as

$$W(s) := \begin{cases} \cos s, & 0 \leq s \leq \pi \\ 0, & \pi \leq s \leq \omega T. \end{cases} \quad (35)$$

Observe that  $W$  has jump discontinuities (of size 1) at all points  $s = n\omega T$  and  $\pi + n\omega T$ ,  $n \in \mathbb{Z}$ , which can be “smoothed out” to obtain to a  $C^k$  version (for any  $1 \leq k \leq \infty$ ) of  $W$  that agrees with the original except on a union of closed intervals containing the discontinuities that is of as small a measure as we wish. Such smoothing may be useful for certain theoretical considerations (as we shall see when it comes to transitions to chaotic dynamics), but we shall not need them for most of our investigation since the map (34) is smooth except on the curves  $\theta + v = 0, \pi$ , which wrap around the cylinder  $\mathbb{S}^1 \times \mathbb{R}$ . When the coefficient of restitution  $e$  is positive, this map has the inverse  $\Phi^{-1} : \mathbb{S}^1 \times \mathbb{R} \rightarrow \mathbb{S}^1 \times \mathbb{R}$  defined as

$$\Phi^{-1}(\theta, v) := (\theta - e^{-1}[v - \gamma W(\theta)], e^{-1}[v - \gamma W(\theta)]), \quad (36)$$

which is also smooth except for a jump discontinuity (of size  $e^{-1}\gamma$ ) in both coordinate functions on curves wrapping around the cylinder.

It should be remarked that we are, just as did Holmes, using the so-called *high-bounce approximation*, which is predicated on the bounces of the ball being significantly higher than the amplitude of oscillation of the floor. Since for tapping the amplitude is zero except for the small time interval of the tap, the approximation is actually exact for most of the motion of the ball, so we expect more accurate results than achieved for steady oscillation of the floor.

Our Holmesian model is clearly a slightly modified version of the *standard map* (cf. [24,27–29]), and one would expect and can actually prove that the multifarious dynamical results proved, illustrated and discussed in [24] for the bouncing ball have analogs for (34). We shall prove and illustrate just a few of these parallels in the sequel, leaving the rest to the interested reader who simply has to follow the course laid out in [24], making the necessary adjustments along the way.

#### 4.1.1. Some elementary dynamical properties of $\Phi$

In the dynamical analysis that follows, we shall assume that  $0 < e < 1$ , which actually corresponds to the most physically realistic case. We begin with an investigation of the fixed points of (34) obtained by solving the equations

$$\begin{aligned} \theta &\equiv \theta + v \pmod{\omega T}, \\ v &= ev + \gamma W(\theta + v), \end{aligned}$$

which lead to the following characterization:

$$\begin{aligned} \llbracket v \rrbracket = 0 &\implies v = m\omega T, \quad m \in \mathbb{Z}, \\ W(\theta) &= \gamma^{-1}(1 - e)v. \end{aligned} \quad (37)$$

From (37) we readily conclude the following: There is always a degenerate family of fixed points – actually a fixed interval –

$$I_{(0)} := (\theta_{(0)}, v_{(0)}) = \{(\theta, 0) : \pi < \theta < \omega T\}, \quad (38)$$

where it is to be understood here and in the sequel that the  $\theta$ -coordinate is always given modulo  $\omega T$ . Then there are isolated pairs of nondegenerate fixed points

$$\begin{aligned} (\theta_{(m)}, v_{(m)}) &= (\cos^{-1}[m\omega T\gamma^{-1}(1 - e)], m\omega T), \\ 1 &\leq |m| \leq M, \end{aligned} \quad (39)$$

for all  $M$  such that

$$1 \leq M \leq \gamma[\omega T(1 - e)]^{-1} = \frac{2a\omega}{g_*T} \left( \frac{1 + e}{1 - e} \right),$$

which could be an empty set.

Next, we determine the (linear) stability of the fixed points. On the interval (38), the derivative of  $\Phi$  (represented as usual as a

matrix in terms of the natural basis for the coordinates  $\theta$  and  $v$ ) is

$$\Phi'(\theta_{(0)}, v_{(0)}) = \begin{pmatrix} 1 & 1 \\ 0 & e \end{pmatrix},$$

so  $I_{(0)}$  is an attracting set. For the additional fixed points (when they exist for  $|m| \geq 1$ ), we compute that

$$\begin{aligned} \Phi'(\theta_{(m)}, v_{(m)}) &= \begin{pmatrix} 1 & 1 \\ \gamma W'(\theta_{(m)}) & e + \gamma W'(\theta_{(m)}) \end{pmatrix} \\ &= \begin{pmatrix} 1 & 1 \\ -\gamma \sin \theta_{(m)} & e - \gamma \sin \theta_{(m)} \end{pmatrix}, \end{aligned}$$

which has eigenvalues

$$\begin{aligned} \lambda_{(m)}^{\pm} &= \frac{1}{2} \left[ (e + 1) - \gamma \sin \theta_{(m)} \right. \\ &\quad \left. \pm \sqrt{((e + 1) - \gamma \sin \theta_{(m)})^2 - 4e} \right], \end{aligned}$$

from which we readily infer the following results regarding the nature of the fixed points and certain associated bifurcations.

**Lemma 2.** *The fixed point  $(\theta_{(m)}, v_{(m)})$  for  $|m| \geq 1$  is a sink if*

$$m\omega T(1 - e) < \gamma < \sqrt{[m\omega T(1 - e)]^2 + (1 + e)^2},$$

*and an orientation-reversing saddle point if*

$$\gamma > \sqrt{[m\omega T(1 - e)]^2 + (1 + e)^2}.$$

Moreover,  $\gamma_k := k\omega T(1 - e)$ , are saddle-node bifurcation values and  $\tilde{\gamma}_k := \sqrt{[k\omega T(1 - e)]^2 + (1 + e)^2}$  are period-doubling (flip) bifurcation values for all  $k \in \mathbb{N}$ .

#### 4.1.2. Attractors and transition to chaos for $\Phi$

Just as in [24], one can show that for  $|m| \geq 1$  each fixed point  $(\theta_{(m)}, v_{(m)})$  gives rise to a period-doubling cascade to chaos as the parameter  $\gamma$  increases across the bifurcation value  $\tilde{\gamma}_m$ . In the process, stable  $2^i$ -cycles give birth to and exchange stability with  $2^{i+1}$ -cycles. Accordingly the map  $\Phi$  has (local) attractors comprised of stable  $2^{k+1}$ -cycles, for any nonnegative integer  $k$  for some parameter interval of the form  $\tilde{\gamma}_k \leq a_k < \gamma < b_k$ . Thus, we see that the map can have cyclic attractors of arbitrarily large period ( $2^i$ ) for the right choices of  $\gamma$  and, again referring to [24], the fact that this period-doubling cascade is an essentially 1-dimensional phenomenon, we can also infer the existence of attracting 3-cycles and other cyclic attractors of arbitrarily large odd periods (cf. [27,28]). In contrast to this kind chaotic behavior, the dynamics for small enough values of  $\gamma$  is quite regular – focused in an attracting spiral – as illustrated in the plot of system iterates in Fig. 1.

For larger  $\gamma$ , one can see, as illustrated by the discrete orbit in Fig. 2, what seems to be a transitional phase from regular to chaotic motion. This transition is manifested by the bifurcation of the fixed point from a spiral sink to a saddle point and the more random appearance of the iterates away from the fixed point. We note that in Figs. 1 and 2 as well as in Figs. 3 and 5, which follow,  $\epsilon$ , denotes the smooth approximation in the model as described above.

There is also another way of showing the existence of an attractor that appears to be *strange* (i.e. is chaotic and has noninteger Hausdorff dimension). This attractor is illustrated in Fig. 3.

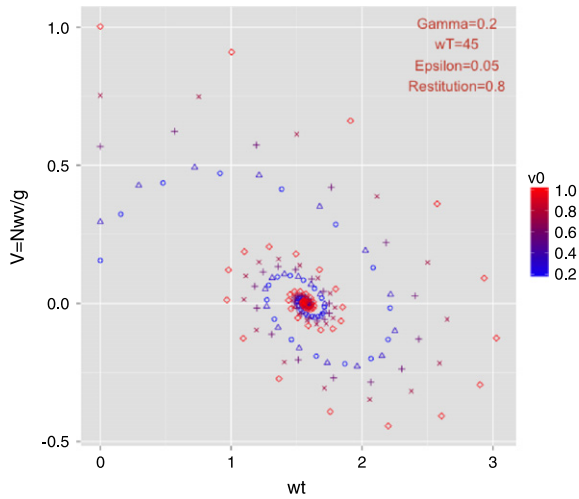


Fig. 1. Regular dynamics for restitution (coefficient)  $e = 0.8$ ,  $\gamma = 0.2$ .

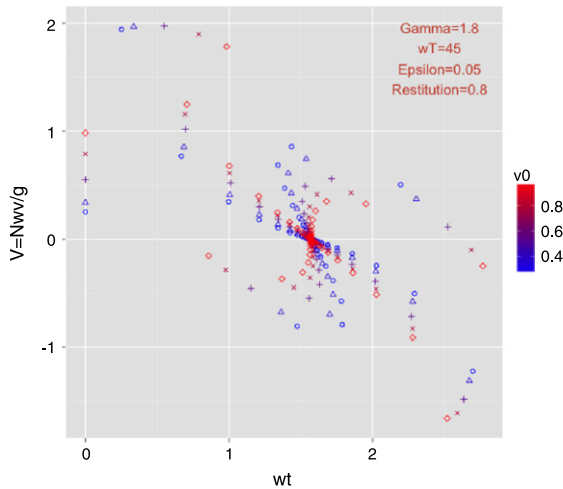


Fig. 2. Transitional dynamics for restitution (coefficient)  $e = 0.8$ ,  $\gamma = 1.8$ .

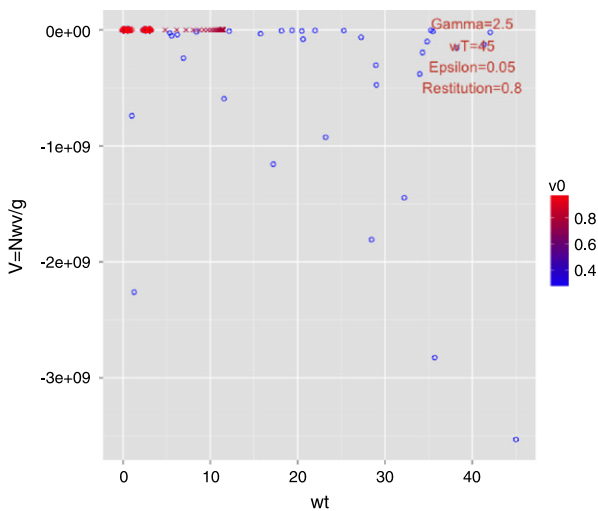


Fig. 3. Possible strange attractor for restitution (coefficient)  $e = 0.8$ ,  $\gamma = 2.5$ .

**Lemma 3.** Let  $\rho$  and  $\gamma$  be such that  $0 < e < 1$ ,  $\omega T(1 - e) < \gamma$  and  $h := \gamma(1 - e)^{-1} \neq m\omega T$  for any  $m \in \mathbb{N}$ . Then

$$\Lambda(\gamma) := \bigcap_{k=1}^{\infty} \Phi^k(R_h),$$

where  $R_h := \{(\theta, v) : |v| \leq h\}$ , is a globally attracting set having a connected component that is an attractor.

**Proof.** It suffices to prove that for any  $(\theta_0, v_0) \in \mathbb{S}^1 \times \mathbb{R}$ ,  $(\theta_n, v_n) := \Phi^n(\theta_0, v_0) \in R_h$  for  $n$  sufficiently large. To this end, we observe that it follows from the definition (34) of  $\Phi$  that

$$|v_n| \leq e|v_{n-1}| + \gamma|W(\theta_{n-1} + v_{n-1})| \leq e|v_{n-1}| + \gamma;$$

whence, we conclude by induction that

$$|v_n| \leq e^n|v_0| + \gamma \sum_{k=0}^{n-1} e^k \leq e^n|v_0| + \gamma$$

for all  $n \in \mathbb{N}$ . Consequently,  $\limsup_n |v_n| \leq h$ . Moreover, since  $|W(\theta_{n-1} + v_{n-1})|$  must actually be zero for some  $n$  we actually can sharpen this result to conclude that  $\limsup_n |v_n| < h$ , which completes the proof.  $\square$

Note that we have refrained from stating that the attractor described by Lemma 2 is strange, even though Fig. 3 certainly strongly indicates that this is the case for  $\gamma$  sufficiently large. The attractor shown is the horizontal Cantor-like set in the upper left-hand corner of the coordinate rectangle, which seems to have a noninteger Hausdorff (fractal) dimension around one. The existence of the strange attractor can in fact be proven and its fractal dimension approximated, but only by a long and arduous – albeit straightforward – argument that we felt was not sufficiently enlightening to be presented here and actually follows directly from a more general result in [38].

We can also prove the existence of full-fledged 2-dimensional horseshoe type chaos associated with transverse homoclinic orbits for  $\gamma$  sufficiently large, which can be seen in the simulation of iterates shown in Fig. 5, which exhibit the type of (seemingly) random splatter pattern indicative of chaotic dynamics. This will be verified geometrically by showing that the map  $\Phi$  behaves locally like a Smale horseshoe map (cf. [24,27,28,39,40]) on a suitably chosen homeomorph of a square contained in  $\mathbb{S}^1 \times \mathbb{R}$ , and it is here that we shall need to consider a smoothed  $C^1$  version of (34). We need only smooth  $W$  in (34), which can be accomplished quite easily by defining for  $0 < \varepsilon \ll \omega T$  the  $C^1$ ,  $\omega T$ -periodic function

$$W_\varepsilon(s) := \begin{cases} -\varepsilon^{-3}(2s - \varepsilon)(s + \varepsilon)^2, & -\varepsilon \leq s \leq 0 \\ \cos s, & 0 \leq s \leq \pi \\ -\varepsilon^{-3}(2s - 2\pi + \varepsilon)(s - \pi - \varepsilon)^2, & \pi \leq s \leq \pi + \varepsilon \\ 0, & \pi + \varepsilon \leq s \leq \omega T - \varepsilon. \end{cases} \quad (40)$$

Note that  $W_\varepsilon$  is a  $C^1$  function with  $W_\varepsilon = W$  except on  $(-\varepsilon, 0) \cup (\pi, \pi + \varepsilon)$  and  $W_\varepsilon \rightarrow W$  as  $\varepsilon \searrow 0$ . Then the corresponding smoothed version of (34) is

$$\begin{aligned} \Phi_\varepsilon : \mathbb{S}^1 \times \mathbb{R} &\rightarrow \mathbb{S}^1 \times \mathbb{R}, \\ \Phi_\varepsilon(\theta, v) &:= (\llbracket \theta + v \rrbracket, ev + \gamma W_\varepsilon(\theta + v)). \end{aligned} \quad (41)$$

Observe that for each admissible  $\varepsilon$  the  $C^1$  version of the map has a couple of additional fixed points for to go along with the fixed points of the original map – one in each of the intervals  $(-\varepsilon, 0)$  and  $(\pi, \pi + \varepsilon)$  – when  $\gamma$  is sufficiently large, but we shall ignore these in the sequel owing to the fact that they are merely artifacts of the  $C^1$  version being used and have no intrinsic role in the dynamics.

**Theorem 1.** Let

$$0 < \varepsilon < \min \left\{ \frac{\omega T}{100}, \frac{(2 - \sqrt{2})(1 + e)(3\pi/4) + (2 + \sqrt{2})(1 - e)\omega T}{2\sqrt{2}(1 + e)} \right\}. \quad (42)$$

Then, if

$$\gamma > 2[(1 + e)(3\pi/4) + (1 - e)\omega T], \quad (43)$$

the map  $\Phi_\varepsilon$  possesses chaotic dynamics of the horseshoe type.

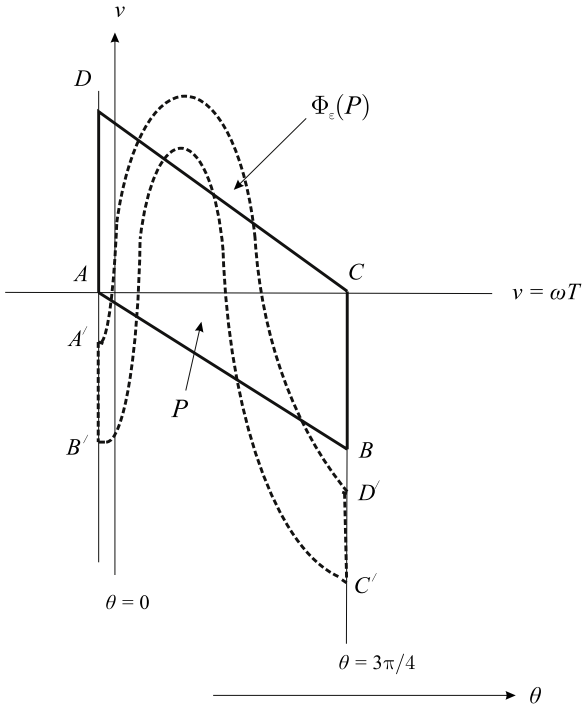


Fig. 4. Horseshoe behavior on  $P$  for  $\gamma$  sufficiently large.

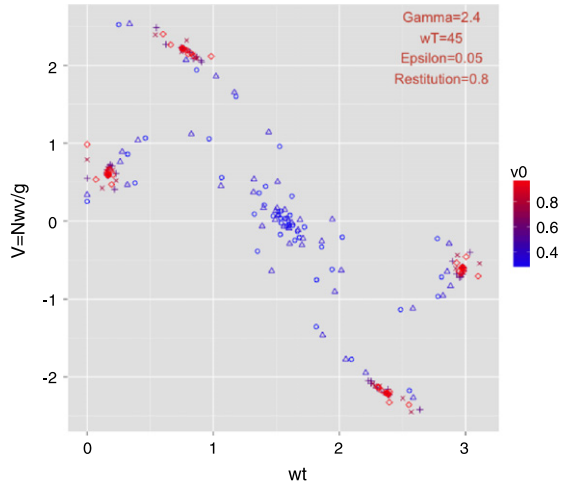


Fig. 5. Chaotic dynamics for restitution (coefficient)  $e = 0.80$ ,  $\gamma = 2.4$ .

**Proof.** We shall show that the hypotheses imply that the restriction of  $\Phi_\varepsilon$  to the parallelogram

$$P := \{(\theta, v) : -2\varepsilon \leq \theta \leq 3\pi/4, -2\varepsilon + \omega T \leq \theta + v \leq (3\pi/4) + \omega T\}$$

behaves like the Smale horseshoe map as illustrated in Fig. 4, so the desired result follows from Moser [39] (cf. Holmes [24]). It is convenient to denote the vertices of  $P$  by  $A := (-2\varepsilon, \omega T)$ ,  $B := (3\pi/4, \omega T - 2\varepsilon - 3\pi/4)$ ,  $C := (3\pi/4, \omega T)$  and  $D := (-2\varepsilon, \omega T + 2\varepsilon + 3\pi/4)$  and the corresponding (straight line segment) edges as  $AB, BC, CD$  and  $DA$ . We note that  $A' := \Phi_\varepsilon(A) = (-2\varepsilon, e\omega T)$ ,  $B' := \Phi_\varepsilon(B) = (-2\varepsilon, e(\omega T - 2\varepsilon - 3\pi/4) - \gamma/\sqrt{2})$ ,  $C' := \Phi_\varepsilon(C) = (3\pi/4, e\omega T - \gamma/\sqrt{2})$  and  $D' := \Phi_\varepsilon(D) = (3\pi/4, e(\omega T + 2\varepsilon + 3\pi/4) - \gamma/\sqrt{2})$ . Observe also that  $\Phi_\varepsilon(AB)$  and  $\Phi_\varepsilon(CD)$  are straight line segments contained in  $\{(\theta, v) : \theta = -2\varepsilon\}$  and  $\{(\theta, v) : \theta = 3\pi/4\}$ , respectively, while  $\Phi_\varepsilon(BC)$  and  $\Phi_\varepsilon(DA)$  are smooth curves ranging from  $\theta = -2\varepsilon$  to  $3\pi/4$ .

As noted above,  $\Phi$  (and a fortiori  $\Phi_\varepsilon$ ) has a fixed point with  $v = \omega T$  and  $\theta \in (0, \pi/2)$  whenever  $\gamma > (1 - e)\omega T$ , which is certainly the case if (43) holds. In order to obtain the desired horseshoe behavior it is necessary for the line segments  $A'B'$  and  $D'C'$  to lie below  $DA$  and  $BC$  along  $\theta = -2\varepsilon$  and  $\theta = 3\pi/4$ , respectively. The first of these requirements is always satisfied in virtue of the definition of  $P$ , while the second property requires that  $D'$  lies below  $B$  along  $\theta = 3\pi/4$ , which is the case if

$$e(\omega T + 2\varepsilon + 3\pi/4) - \gamma/\sqrt{2} < \omega T - 2\varepsilon - 3\pi/4.$$

But this inequality is readily seen to be equivalent to

$$\gamma > \sqrt{2}[(1 + e)(2\varepsilon + 3\pi/4) - (1 - e)\omega T],$$

which is clearly implied by (42) and (43), so we do have the necessary positioning of  $A'B'$  and  $D'C'$ .

At this stage, it remains only to prove that the hypotheses guarantee that the curve  $\Phi_\varepsilon(BC)$  lies above the edge  $CD$  for some value of  $\theta$  in the interval  $(0, \pi/2)$ . Toward this end, it is easy to show that  $\Phi_\varepsilon(BC)$  is just the graph of the function

$$v = \varphi(\theta) := e(\theta + \omega T - 3\pi/4) + \gamma W_\varepsilon(\theta)$$

on the interval  $-2\varepsilon \leq \theta \leq 3\pi/4$ , which obviously must achieve its maximum for  $\theta \in (0, \pi/2)$ , and this by definition occurs when  $e - \gamma \sin \theta = 0$ .

Denoting this maximizer by  $\theta_M$ , we require that

$$\theta_M + v(\theta_M) > \omega T + 3\pi/4,$$

which is equivalent to

$$e(\theta_M + \omega T - 3\pi/4) + \gamma\sqrt{1 - (e/\gamma)^2} > \omega T + 3\pi/4,$$

and this is the same as

$$\gamma\sqrt{1 - (e/\gamma)^2} > (1 + e)(3\pi/4 - \theta_M) + (1 - e)\omega T.$$

But this inequality follows directly from (43), so the proof is complete.  $\square$

Chaotic dynamics indicated by a seemingly random scattering (or splatter), albeit a bit sparse, of the iterates is shown in Fig. 5.

## 5. Comparison with simulations

In this section, results of discrete element simulations are presented that support the findings in the theory with regard to periodic and chaotic behavior of the column mass center. In particular, we consider a system of uniform spheres (diameter  $d$  and mass  $m$ ) that are subjected to discrete taps applied to the floor in the form of half sine displacements of amplitude  $a/d$  and  $f$ . The taps are separated by a fixed relaxation interval denoted as  $\tau_r$ . Various behavioral regimes (periodic to chaotic) are realized by fixing one tap parameter (either  $a/d$  or  $f$ ) while varying the other. We remark that the appearance of these regimes is very much dependent on the relaxation interval  $\tau_r$  from the viewpoint that in the limit of  $\tau_r \rightarrow 0$ , the dynamics become chaotic. We have carried out a series of preliminary cases in which  $a/d$  and  $f$  were fixed and the relaxation time was varied.

The simulation method entails numerical integration (via a velocity Verlet leap-frog method) of Newton's equations for the system of interacting spheres, where the quasi-static force model follows the Walton-Braun soft sphere model [2,41]. Here, the normal impulse acting between contacting particles is a function of an allowed overlap  $\alpha$ , loading through a linear spring of stiffness  $K_1$  and unloading with stiffness  $K_2$  such that  $K_1 < K_2$ . The model admits a constant restitution coefficient  $e := \sqrt{K_1/K_2}$ . The value of  $K_1$  is selected so as to ensure that  $\alpha < 0.01d$ . This quasi-static

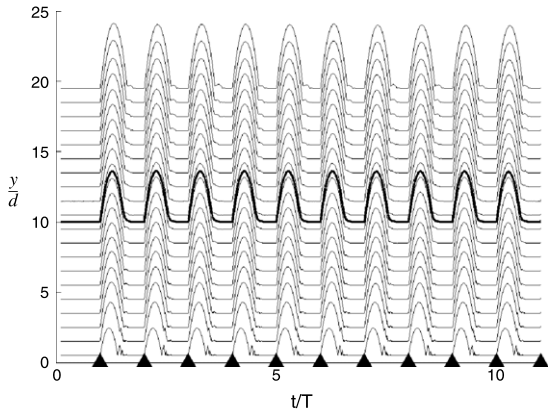


**Fig. 6.** Trajectories of the sphere centers and the mass center (dark line) for  $\tau_r = 0.4$ ,  $f = 10$  Hz and  $a/d = 0.50$  over the first 10 taps. Triangles on the time axis indicate when the tap was applied.

model is applicable because the wave speed in the material is much larger than the duration of contacts between the spheres. Since the objective of these simulations was simply to examine the mass center dynamics, we limited the magnitude of the tap velocity so that it was not necessary to incorporate a velocity-dependent restitution coefficient. The integration time step  $\Delta t \cong 10^{-8}$  s is approximately three orders of magnitude less than the usual value as determined by the duration of loading ( $\Delta t \sim \sqrt{m/K_1} \cong 10^{-5}$  s).

The column consisted of 20 spheres, each having a mass density  $\rho = 1200$  kg/m<sup>3</sup> and  $e = 0.9$  in reasonably good agreement with experimental measurements [42]. For all studies, a fixed relaxation interval  $\tau_r = 0.4$  s was used, and  $T := (f/2) + \tau_r$  was used to normalize time  $t$  in the mass center trajectory plots. The following twelve case studies were completed:  $a/d = 0.5$ , with  $f = 5, 10, 15, 20, 25, 30$  Hz; and  $f = 10$  Hz, with  $a/d = 0.25, 0.50, 0.75, 1.0, 1.25, 1.50$ . Figs. 6–8 show the trajectories of the particles for the first 10 taps (normalized by  $d$ ), and the mass center (dark lines) for  $f = 10$  Hz and  $a/d = 0.50, 0.75, 1.50$ . The small triangles on the abscissa represent the time when the tap was applied. For  $a/d = 0.50$  (Fig. 6), the mass center executes periodic motion as the time between taps ( $\tau_r$ ) is of sufficient duration to allow the system to relax. Consequently, each sphere in the system has a comparable trajectory, except for that adjacent to the floor, which experiences two bounces due to collisions with the particle above it. For a larger amplitude  $a/d = 0.75$  (Fig. 7), the mass center appears to undergo a period doubling motion; and at  $a/d = 1.50$ , the mass center trajectory does not feature any periodicity. In extended case studies, 100 taps were applied to the system during which the mass center trajectories shown in Figs. 6–8 persisted.

The behavior of the mass center for fixed  $a/d$  and varying frequency was analogous in that larger frequencies produced chaotic trajectories as can be seen in Fig. 9, where  $a/d = 1$  and  $f = 15$  Hz. However, some counterintuitive trends were observed, such as in Fig. 10 ( $a/d = 1$  and  $f = 20$  Hz) where the trajectory appears to be periodic. A more complete picture of the dynamics for the case  $f = 10$  Hz is presented in Fig. 11, which shows a Poincaré map of the mass center trajectory at  $t = T$  as a function of  $a/d$ . Note that this Poincaré map also plays the role of a bifurcation diagram. Here, one observes periodic, period-doubling and chaotic dynamics for which several individual trajectories were shown in Figs. 6–8.

It is instructive to make some comparisons of the simulation results with our analytical investigations in Sections 3 and 4. Of course, we need to point out that the force models described in Sections 2–4 use (in aid of simplifying the analysis) slightly different interaction force models from those employed in the simulations. However, one can show that the differences

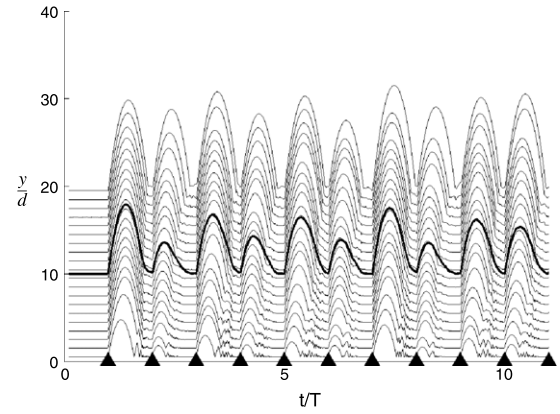


**Fig. 7.** Trajectories of the sphere centers and the mass center (dark line) for  $\tau_r = 0.4$ ,  $f = 10$  Hz and  $a/d = 0.75$  over the first 10 taps. Triangles on the time axis indicate when the tap was applied.

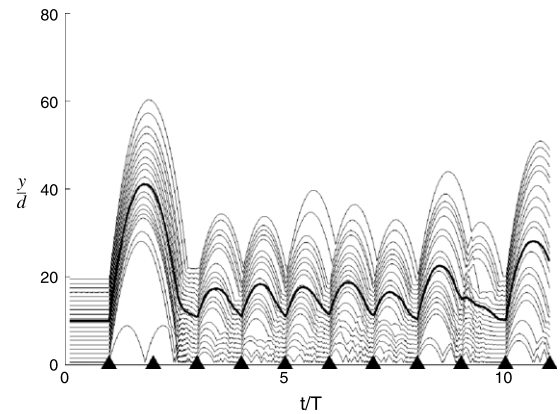


**Fig. 8.** Trajectories of the sphere centers and the mass center (dark line) for  $\tau_r = 0.4$ ,  $f = 10$  Hz and  $a/d = 1.50$  over the first 10 taps. Triangles on the time axis indicate when the tap was applied.

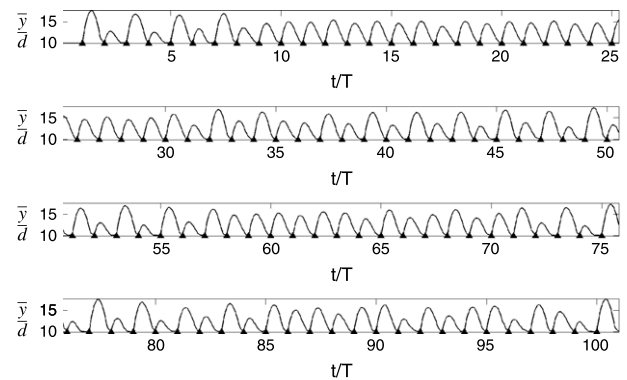


**Fig. 9.** Mass center trajectory over 100 taps for  $a/d = 1$  and  $f = 15$  Hz.

in the dynamics for any of these interaction models should be insignificant, so comparisons between the simulations and analytical results are quite meaningful. The first thing that one notices in Figs. 6–8 is that the trajectory of the particle nearest the floor tends to be the most complicated of all the elements in the configuration, which is not surprising since it takes the brunt of the taps and is subjected to collisions with the remainder of the stack. In particular, it can be seen that the motion of the lowest particle does not conform to a key approximation – namely the one used to obtain (29) – except perhaps on average. Presumably, if the number of particles was considerably greater, better agreement with the assumption regarding the relationship between the orbits

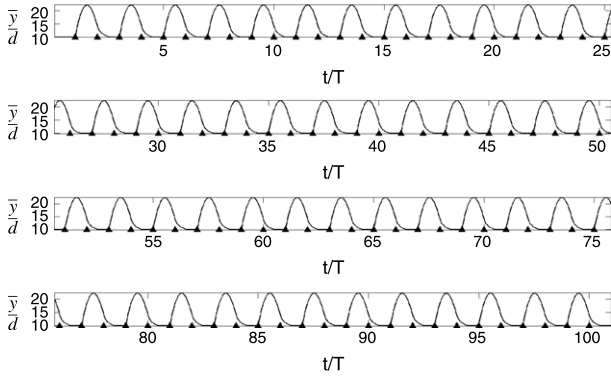


Fig. 10. Mass center trajectory over 100 taps for  $a/d = 1$  and  $f = 20$  Hz.

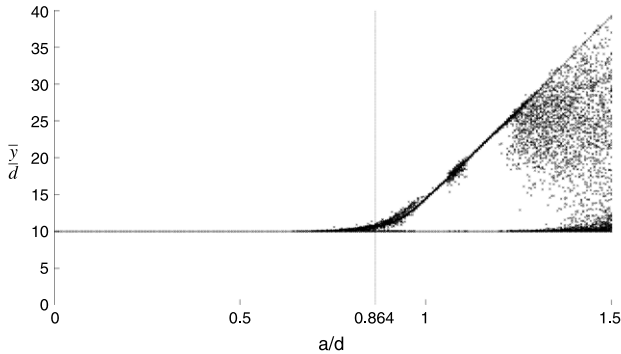


Fig. 11. Poincaré map of mass center trajectory at  $t = T$  as a function of  $a/d = 1$  for  $f = 10$  Hz.

of the lowest particle and the mass center would be realized. Nevertheless, these same simulations do tend to support the value of the mass center dynamics as an indicator of the overall system dynamics, especially with regard to transitions to chaos. One can see this most clearly by noting how the qualitative dynamics of the mass center mirrors that of just about all the individual particles.

For example, the apparent periodicity of the mass center in the simulation pictured in Fig. 6 seems to be replicated by trajectories of all twenty balls in the configuration. In addition, what appears to be period doubling in the orbit of the mass center in Fig. 7 seems also to characterize the trajectories of all except for the three or four lowest particles in the stack over the whole tapping sequence and possibly all the balls after sufficiently many taps. On the other hand, the simulation for the case depicted in Fig. 8, which corresponds to the largest value of the fundamental dimensionless parameter  $\gamma$  of (34), indicates that the apparent chaos of the trajectory of the mass center reflects what seem to be chaotic trajectories of all the balls – with balls nearest the floor (as one might expect) manifesting the most complicated orbits.

The simulations illustrated in Figs. 6–9 all show a trend toward more complex orbit structure and ultimately prevalent chaotic regimes as the parameter  $\gamma$  increases, which agrees quite nicely with the analysis of the approximate discrete model studied in Section 4. This behavior is also in excellent agreement with the experiments performed in Lumay et al. [11]. Apart from suggesting that our discrete model (34) is a reasonably useful tool for predicting the evolution of the full tapping system, this indicates that the single parameter  $\gamma$  provides a rather useful measure of the dynamics of the system. Moreover, our discrete model can also be used to explain the apparent “outlier” illustrated in Fig. 10, for Lemma 2 shows that there are parameter intervals (or windows) corresponding to arbitrarily large values of  $\gamma$  for which (34) has a sink, which corresponds to a stable periodic orbit.

## 6. Visualization analysis

We offer in this section a refined visual analysis of the discrete Holmes-type model introduced in Section 4 to complement the analytical results established previously and provide further insight into the qualitative properties of our model. The objective in providing additional modes of visualizing the dynamics is to reveal more of the inherent topological structures present in the  $(\theta, v)$  phase portrait of the discrete dynamical system associated with  $\Phi$ . In short, application of a variety of visualization techniques often enhances one’s understanding of subtle topological characteristics (such as coherent structures) of the dynamics that can escape more basic renderings and even some analytical investigations. Specifically, we introduce in the following an enhanced version of the standard scatter plot technique used to visualize discrete dynamical systems that yields a denser, more textured sampling of the phase portrait. Corresponding results are subsequently presented for a range of  $\gamma$  values in the definition the dynamical system  $\Phi$  and observations are made about the properties and structures that these representations reveal.

In addition to enhanced discrete renderings and interpolation methods, we briefly describe an averaging technique that often provides topological insights to the dynamics.

### 6.1. Enhanced scatter plot

The most straightforward way to represent a discrete dynamical system consists in plotting the successive states of the system corresponding to a set of initial conditions. By assigning different colors to different initial conditions, individual orbits may be inferred from the resulting plot. Figs. 1–3 show the results produced by this technique. A high-resolution visualization of the dynamics usually requires the use of a larger number of initial conditions. While this approach increases the spatial resolution of the plot, it also tends to create a cluttered representation, unless the system exhibits a quasi-periodicity, thus allowing the discrete plot to densely populate the underlying manifolds of the topology (stable, unstable, KAM tori, Cantori).

Specifically, each plot is comprised of points defined as follows.

$$(\mathbf{x}_i^j)_{0 \leq i \leq M, 1 \leq j \leq N}, \quad \text{with } \mathbf{x}_i^j := (\theta_i^j, v_i^j) \text{ and } \mathbf{x}_{i+1}^j = \Phi(\mathbf{x}_i^j),$$

and the initial conditions  $\mathbf{x}_0^j$ ,  $1 \leq j \leq N$  are distributed over some region  $D \subset [0, \omega T] \times \mathbb{R}$ .

In the absence of quasi-periodicity (which is typically the case for non-conservative systems, such as  $\Phi$  when  $e < 1$ ), an alternative approach consists in fitting an interpolating curve through the successive states of the system to produce a continuous approximation of the discrete orbit (thereby implicitly assuming the presence of an underlying manifold). Using the notations introduced above, one defines for each initial condition  $\mathbf{x}_0^j$  a smooth curve  $\mathbf{s}_j : I \subset \mathbb{R} \rightarrow \mathbb{R}^2$ , that satisfies the interpolating conditions

$$\forall i \in [1, M], \quad \exists t \in I \subset \mathbb{R}, \quad \mathbf{s}_j(t) = \mathbf{x}_i^j.$$

In the results presented below, two types of interpolation are considered. The first one is a piecewise linear function, while the second corresponds to a cardinal (or canonical) spline that yields a smooth interpolating curve.

A comparison among the results produced by these different methods is presented in Fig. 12.

#### 6.1.1. Orbit averaging

While the curve interpolation of discrete points offers a visual approximation of a putative underlying manifold, it can produce

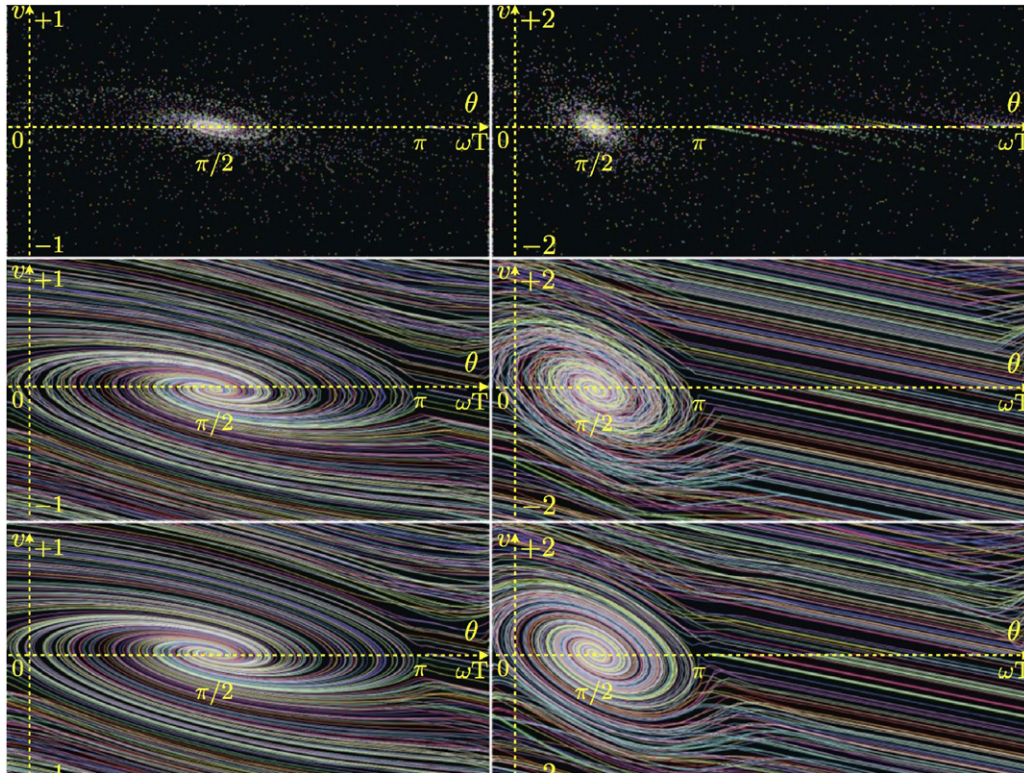


**Fig. 12.** Dense visualization of discrete dynamical system  $\Phi$  for  $\gamma = 0.1$  (left) and  $\gamma = 0.5$  (right). *Top row:* discrete scatter plot. *Middle row:* Piecewise linear interpolation of individual orbits. *Bottom row:* Smooth interpolation of individual orbits using splines. The attractor at  $(\frac{\pi}{2}, 0)$  is clearly visible in each representation.

strong artifacts since the interpolation method (in our case cardinal splines) is oblivious to the actual constraints of the system. We have recently proposed a method specifically designed for discrete dynamical systems that addresses this problem through a massively parallel computation [35]. The basic idea of this method consists in assigning a random color to each pixel of an image that covers the considered region of the phase portrait and then assigning to each pixel of the output image the color corresponding to the average color of the pixels sampled by the orbit that was initiated at that location. In effect, this method applies a low-pass filter to the image along a subset of pixels that is restricted to individual orbits. Hence the method produces patterns that show the underlying manifolds and various other invariant sets as streaks of nearly uniform color. As a result, orbit averaging techniques usually reveal more of the orbit topology and especially boundaries separating different types of dynamical regimes.

## 6.2. Visualization results

The methods described above has been applied to the discrete dynamical system defined in Eq. (34) for various parameterizations of the system. In all experiments, the following constant values are used:  $a = 0.1$ ,  $e = 0.8$ ,  $N = 20$ , and  $T = 10$ . In contrast, the value of the parameter  $\gamma$  varies in the interval  $[0.1, 4.0]$  and the value of  $\omega$  is adjusted accordingly. Note that the value for  $T$  was chosen to satisfy  $\pi < \omega T$ , thus ensuring that the relaxation interval  $[\pi, \omega T]$  is non-empty and the function  $y$  is continuous.

We consider the spline interpolation method for values of  $\gamma$  ranging from 0.1 to 4.0. As previously noted, variations of  $\gamma$  in this interval induce a transition from regular dynamics to chaos. Corresponding results are shown in Fig. 13. Observe that the portion of the phase portrait visible in those images is restricted to the interval  $\theta \in [0, \pi]$  since the dynamics is linear by construction outside of that region.

As mentioned previously, the spline interpolation approach implicitly assumes the existence of one-dimensional manifolds underlying the geometry of individual orbits. This strategy significantly improves the visualization of regular dynamics, as can be seen by comparing the images in Fig. 14 with Fig. 13.

However, as the dynamics transitions to chaos, the spline model proves less suitable and tends to produce ambiguous results: while the bottom center and right images in Fig. 14 clearly reveal what appears as a period-doubling bifurcation, the corresponding images in Fig. 13 are more ambiguous. In particular, the presence of several attractors is not readily apparent in the last image in Fig. 13.

An example of orbit averaging is shown in Fig. 15. This does provide an enhanced understanding of the topological aspects of the dynamics in several ways. For example, Fig. 15 indicates that the distributions of the spiral orbits around fixed points tend to be quite uniform. Moreover, we see that the spirals are enclosed in strips bounded by what appear to be thickened curves indicating coherent structures of some kind (perhaps separatrices) that divide distinctly different types of dynamical behavior.

## 7. Concluding remarks and future research

Our focus in this research is the dynamics of a (one-dimensional) vertical column of particles in the presence of gravity and resting on a floor that is subject to periodic (impulse-like) tapping, where we have assumed realistic, nonlinear particle–particle and particle–floor interaction forces of a simplified Walton–Braun type. The primary goal was to show that there are mathematically tractable reductions that can serve as fairly reliable indicators of certain aspects of the dynamics of the entire system. In particular, we investigated the motion of the center of mass of the particle configuration knowing that among other things, it should serve well as a marker for transitions from regular to chaotic dynamics for the entire system. We showed, starting with a classical Newtonian model for the motion of the column of particles, that with a

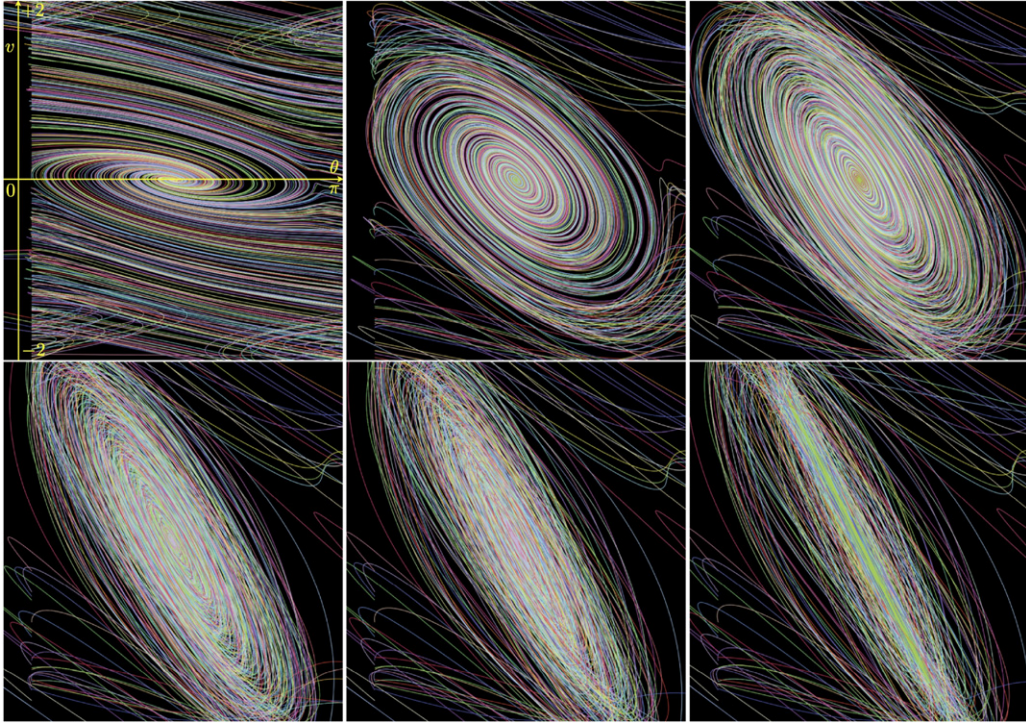


**Fig. 13.** Transition to chaos in Holmes-type dynamical system  $\Phi$ . The individual images correspond to  $\gamma = 0.1, 1.0, 2.0, 3.0, 3.5,$  and  $4.0$ , respectively.

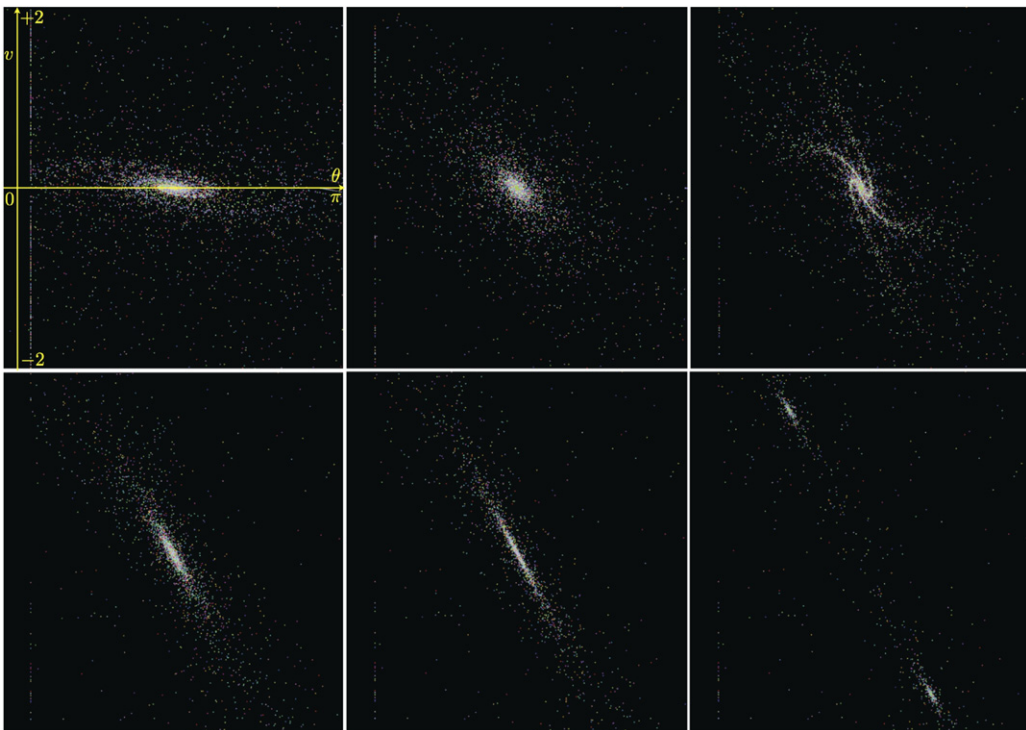


**Fig. 14.** Transition to chaos in Holmes-type dynamical system  $\Phi$ . The individual images correspond to  $\gamma = 0.1, 1.0, 2.0, 3.0, 3.5,$  and  $4.0$ , respectively.

very plausible assumption concerning the trajectory of the particle closest to the floor, the center of mass dynamics is essentially equivalent to that of a single more massive particle (ball) bouncing on the periodically tapped floor; a significant dynamical reduction that opened several simpler avenues of mathematical analysis.

Naturally, the approximate equivalence with the motion of a single ball on an oscillating plate leads to direct connections with the wealth of bouncing ball literature such as in [23–26].

Furthermore, we were able to exploit the bouncing ball analog to obtain à la Holmes [24] an approximate two-dimensional discrete dynamical model – similar to the standard map – of the tapped motion of the center of mass; a model that we were able to analyze in considerable detail. This analysis uncovered the existence of period doubling routes to chaos, Smale horseshoe chaos and the existence of interesting, apparently strange, attractors. Moreover, we were able to identify a key dimensionless parameter, namely  $\gamma$ ,

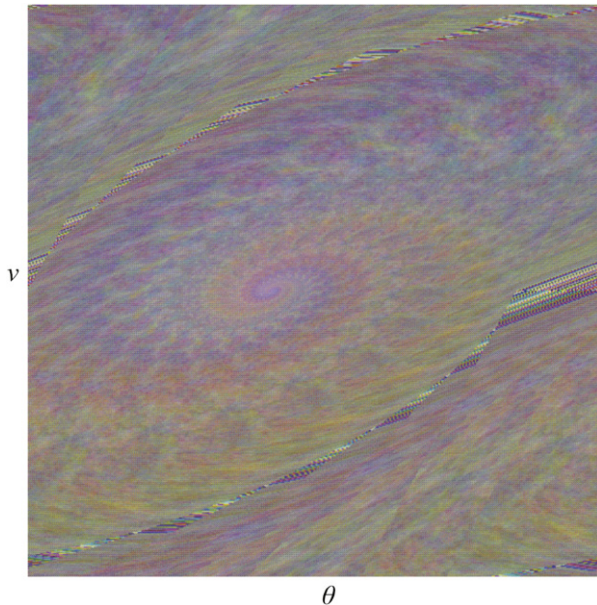


Fig. 15. Orbital averaging for  $T = 10$  (50 iterations).  $\gamma = 0.1$ ,  $-1 \leq v \leq 5$ .

related directly to the impulse energy of the taps and coefficients of restitution of the material interactions that serves as the central bifurcation parameter for the dynamics.

Our overall strategy for investigating granular flows is comprised of three complementary components: modern dynamical systems theory based analysis; simulation employing a sophisticated molecular dynamics based code capable of dealing with the motion of thousands of particles; and the use of advanced computer assisted dynamical visualization techniques that can render graphical images that can illustrate important features of flows with remarkable clarity and precision. Accordingly the analysis of the reduced dynamical system for the motion of the center of mass of the column of particles was also tested for effectiveness by comparison with simulation and visualization studies. For the simulations, extensive computations were done for large numbers of particles with various properties and the corresponding center of mass dynamics for a rather wide range of tapping processes. The results of virtually all of these simulations, several of which are illustrated in the paper, confirm the effectiveness of the center of mass reduction in predicting the onset of chaos and also indicating other dynamical features such as the identification of the key dimensionless bifurcation parameter. In addition, many of the results obtained from analyzing the reduced dynamical model agree quite well with our recent stochastic and discrete element findings on density relaxation [7,15,31].

We also compared the reduced dynamical systems analysis with a study of the associated single ball dynamics using some of the powerful visualization techniques that have been developed in recent years (see e.g. [32–35]). The results of this comparison were also quite good. In particular, the single ball visualizations indicated a very strong correlation with the discrete dynamical system approximation dynamics, and so all three components of our approach seemed to be in mutual agreement with regard to the dynamical predictions for the tapping problem investigated, which is a first step in what we believe should be a harmonious three-pronged approach to investigating a much wider range of granular flow systems.

As for related future research, Figs. 6–11, and Fig. 11 in particular, indicate that it might be worthwhile to try to find an alternative discrete dynamical system model for the motion of the mass center – a (planar) *stroboscopic map* that gives the position and velocity at times  $t = T, 2T, 3T, \dots$ . This is something we

are now working on. Moreover, the reduction results obtained for the one-dimensional tapping problem suggest some higher dimensional generalizations. For example, if one taps a two- or three-dimensional container of particles, it may be possible to obtain some information on the overall dynamics by investigating the motion of the center of mass of horizontal layers of the particle configurations. And if the container has a plane or axis of symmetry, the reduced system is apt to be just as tractable mathematically as the one-dimensional particle configuration investigated in this paper. We intend to look into this in the near future.

## Acknowledgments

D. Blackmore's, A. Rosato's and X. Tricoche's work in this paper was supported in part by NSF Grant CMMI-1029809. The authors also thank the reviewers for constructive criticism that contributed to this improvement of our original manuscript.

## References

- [1] D. Blackmore, A. Rosato, X. Tricoche, K. Urban, V. Ratnaswamy, Tapping dynamics for a column of particles and beyond, *JOMMS* 6 (2011) 71–86.
- [2] O.R. Walton, R.L. Braun, Stress calculations for assemblies of inelastic spheres in uniform shear, *Acta Mech.* 63 (1–4) (1986) 73–86.
- [3] O.R. Walton, R.L. Braun, Simulation of rotary-drum and repose tests for frictional spheres and rigid sphere clusters, in: *Joint DOE/NSF Workshop on Flow of Particulates and Fluids*, Ithaca, NY, 1993.
- [4] A. Alexeev, A. Goldshtein, M. Shapiro, The liquid and solid states of highly dissipative vibrated granular columns: one-dimensional computer simulations, *Powder Technol.* 123 (2002) 83–104.
- [5] D. Blackmore, R. Dave, Chaos in one-dimensional granular flows with oscillating boundaries, in: R. Behringer, J. Jenkins (Eds.), *Powders & Grains 97*, Balkema, Rotterdam, 1997, pp. 409–412.
- [6] C. Daraio, V. Nesterenko, E. Herbold, S. Jin, Tunability of solitary wave properties in one dimensional strongly nonlinear phononic crystals, *Phys. Rev. E* 73 (2006) 026610.
- [7] O. Dybenko, A. Rosato, D. Hornthrop, Monte Carlo modeling of density relaxation induced by energetic taps, *Kona Particle and Powder* 25 (2007) 133.
- [8] E. Falcon, C. Laroche, S. Fauve, C. Coste, Collision of a 1-D column of beads with a wall, *Eur. Phys. J. B* 5 (1998) 111–131.
- [9] G. Friesecke, J. Wattis, Existence theorem for solitary waves on lattices, *Comm. Math. Phys.* 161 (1994) 391–418.
- [10] J. Hong, J.-Y. Ji, H. Kim, Power laws in nonlinear chains under gravity, *Phys. Rev. Lett.* 82 (1999) 3058–3061.
- [11] G. Lumay, S. Darbolo, O. Gerasymov, N. Vanderwalle, Experimental study of a vertical column of grains submitted to a series of impulses, *Eur. Phys. J. E* 36 (2013) 13016.
- [12] V. Nesterenko, Propagation of nonlinear compression pulses in granular media, *J. Appl. Mech. Tech. Phys.* 24 (1984) 733–743.
- [13] M. Porter, C. Daraio, I. Szelengowicz, E. Herbold, P. Kevrekidis, Highly nonlinear solitary waves in heterogeneous periodic granular media, *Physica D* 238 (2009) 666–676.
- [14] P. Poggi, S. Ruffo, Exact solutions in FPU oscillator chain, *Physica D* 103 (1997) 251–272.
- [15] A. Rosato, O. Dybenko, V. Ratnaswamy, D. Hornthrop, L. Kondic, Microstructure development in tapped granular systems, *Phys. Rev. E* 81 (2010) 061301.
- [16] S. Sen, M. Manciu, Discrete Hertzian chains and solitons, *Physica A* 268 (1999) 644–649.
- [17] S. Sen, M. Manciu, Solitary wave dynamics in generalized Hertz chains: an improved solution of the equation of motion, *Phys. Rev. E* 64 (2001) 056605-1–056605-4.
- [18] J. Wakou, A. Ochiai, M. Isobe, A Langevin approach to one-dimensional granular media fluidized by vibrations, *J. Phys. Soc. Japan* 77 (2008) 034402. 5 pages.
- [19] R. Yang, J. Wylie, Degenerate orbit transitions in a one-dimensional inelastic particle system, *Phys. Rev. E* 82 (2010) 011302.
- [20] S. Luding, *Studies of Columns of Beads under External Vibrations*, Ph.D. Thesis, Universität Freiburg, Oct. 1994.
- [21] S. Luding, E. Clement, A. Blumen, J. Rajchenbach, J. Duran, Studies of columns of beads under external vibrations, *Phys. Rev. E* 49 (1994) 1634.
- [22] C. Brennen, S. Ghosh, C. Wassgren, Vertical oscillation of a bed of granular material, *Trans. ASME* 63 (1996) 156–161.
- [23] T. Gilet, N. Vandewalle, S. Darbolo, Completely inelastic ball, *Phys. Rev. E* 79 (2009) 055201(R).
- [24] P. Holmes, The dynamics of repeated impacts with a sinusoidally vibrating plate, *J. Sound Vib.* 84 (2) (1982) 173–189.

- [25] T. Mello, N. Tuffillaro, Strange attractors of a bouncing ball, *Am. J. Phys.* 55 (1987) 316–319.
- [26] S. Vogel, S. Linz, Regular and chaotic dynamics in bouncing ball models, *Int. J. Bifurc. & Chaos* 21 (2011) 869–884.
- [27] J. Guckenheimer, P. Holmes, *Nonlinear Oscillations, Dynamical Systems, and Bifurcations of Vector Fields*, Springer-Verlag, New York, 1983.
- [28] A. Katok, B. Hasselblatt, *Introduction to the Modern Theory of Dynamical Systems*, Cambridge University Press, Cambridge, 1995.
- [29] J. Meiss, Visual explorations of dynamics: the standard mapping, *Pramana - J. Phys. Indian Acad. Sci.* 70 (2008) 965–988.
- [30] V. Ratnaswamy, A. Rosato, D. Blackmore, X. Tricoche, N. Ching, L. Zuo, Evolution of solids fraction surfaces in tapping: simulation and dynamical systems analysis, *Granular Matter* 14 (2012) 169–174.
- [31] A. Rosato, V. Ratnaswamy, D. Hornthrop, O. Dybenko, L. Kondic, Temporal dynamics in density relaxation, in: *Proc. Joint IUTAM-ISIMM Sympos. on Mathematical Modeling and Physical Instances of Granular Flows*, Reggio-Cabria, Italy, 14–18 Sept. 2009, AIP Conference Proceedings 1227, pp. 89–99.
- [32] G. Haller, Distinguished material surfaces and coherent structures in three-dimensional flows, *Physica D* 149 (2001) 248–277.
- [33] T. Lindeberg, Edge detection and ridge detection with automatic scale selection, *Int. J. Comput. Vis.* 30 (1998) 117–156.
- [34] N. Max, B. Becker, *Flow Visualization Using Moving Textures*, NASA Conference Publication, 1996, pp. 77–88.
- [35] X. Tricoche, C. Garth, A. Sanderson, Visualization of topological structures in area-preserving maps, *IEEE Trans. Visual. Comput. Graphics* 17 (2011) 1765–1774.
- [36] R. MacKay, Solitary waves in a chain of beads under Hertz contact, *Phys. Lett. A* 251 (1999) 191–192.
- [37] A. Lazer, S. Solimini, On periodic solutions of nonlinear differential equations with singularities, *Proc. Amer. Math. Soc.* 99 (1987) 109–114.
- [38] Y. Joshi, D. Blackmore, Strange attractors for asymptotically zero maps. arXiv:1310.5417 [math.DS].
- [39] J. Moser, *Stable and Random Motion in Dynamical Systems*, Princeton University Press, 1973.
- [40] S. Smale, *The Mathematics of Time*, Springer-Verlag, New York, 1980.
- [41] O.R. Walton, Numerical simulation of inclined chute flows of monodisperse, inelastic, frictional spheres, *Mech. Mater.* 16 (1993) 239–247.
- [42] M.Y. Louge, Impact Parameter Chart for Spheres, 1999. Available from: <http://grainflowresearch.mae.cornell.edu/impact/data/Impact%20Results.html>.